ACS Chemical Neuroscience

Research Article

pubs.acs.org/chemneuro

Synthesis and Evaluation of [^{18}F]RAGER: A First Generation Small-Molecule PET Radioligand Targeting the Receptor for Advanced Glycation Endproducts

Brian P. Cary,[†] Allen F. Brooks,[†] Maria V. Fawaz,[†,‡] Lindsey R. Drake,[‡] Timothy J. Desmond,[†] Phillip Sherman,[†] Carole A. Quesada,[†] and Peter J. H. Scott*[,†,‡]

[†]Division of Nuclear Medicine, Department of Radiology, University of Michigan Medical School, Ann Arbor, Michigan 48109, United States

[‡]The Interdepartmental Program in Medicinal Chemistry, University of Michigan, Ann Arbor, Michigan 48109, United States

Supporting Information

ABSTRACT: The receptor for advanced glycation endproducts (RAGE) is a 35 kDa transmembrane receptor that belongs to the immunoglobulin superfamily of cell surface molecules. Its role in Alzheimer's disease (AD) is complex, but it is thought to mediate influx of circulating amyloid-β into the brain as well as amplify Aβ-induced pathogenic responses. RAGE is therefore of considerable interest as both a diagnostic and a therapeutic target in AD. Herein we report the synthesis and preliminary preclinical evaluation of [^{18}F]RAGER, the first small molecule PET radiotracer for RAGE (K_d = 15 nM). Docking studies proposed a likely binding interaction between RAGE and RAGER, [^{18}F]RAGER autoradiography showed colocalization with RAGE identified by immunohistochemistry in AD brain samples, and [^{18}F]RAGER microPET confirmed CNS penetration and increased uptake in areas of the brain known to express RAGE. This first generation radiotracer represents initial proof-of-concept and a promising first step toward quantifying CNS RAGE activity using PET. However, there were high levels of nonspecific [^{18}F]RAGER binding *in vitro*, likely due to its high log *P* (experimental log *P* = 3.5), and rapid metabolism of [^{18}F]RAGER in rat liver microsome studies. Therefore, development of second generation ligands with improved imaging properties would be advantageous prior to anticipated translation into clinical PET imaging studies.

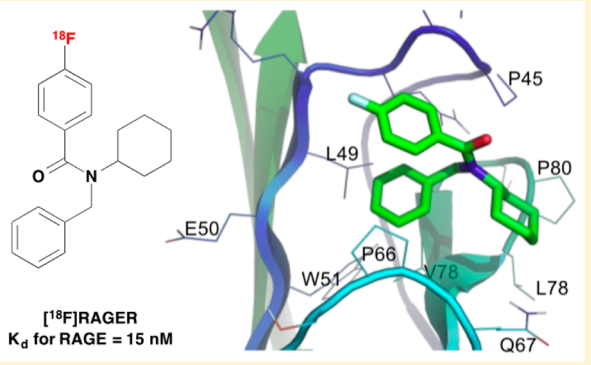

KEYWORDS: *RAGE, radiotracer, positron emission tomography, fluorine-18*

Positron emission tomography (PET) is a powerful functional imaging technique for examining neurobiological parameters *in vivo*. Its use for clinical Alzheimer's disease (AD) research is extensive, focusing initially on the quantification of insoluble protein aggregates that accumulate in AD. Most efforts have concentrated on developing radiotracers to image β-amyloid (Aβ) deposits, and notable probes in this category include AMYViD ([^{18}F]AV-45), Neuraceq, Vizamyl, and [^{11}C]Pittsburgh compound B ([^{11}C]-PiB).[1−3] More recently, focus has shifted to development of radiotracers that can quantify tau neurofibrillary tangles.[4] The ability to quantify the pathology of amyloid and tau formation in AD will be critical in the development of disease modifying therapies for these targets. However, imaging these protein aggregates is only part of the story[5,6] because they represent only two components of a complex and lengthy cascade. While the role of amyloid and tau in AD pathology is increasingly understood, the entire AD cascade that ultimately leads to severe cognitive decline remains ambiguous. When this gap in knowledge is considered along with the immense socio-economic burden of AD,[7,8] the urgent need for a series of PET radioligands to better understand the entire pathway of AD progression and support AD therapeutic development efforts is apparent (for recent perspectives on other potential imaging targets in AD, see refs 9 and 10). To this end, our laboratory and others have been working extensively to develop PET probes relevant to AD outside the scope of traditional Aβ targeting, such as radioligands with affinity for metal−Aβ species,[11,12] glutaminyl-cyclase,[13] and glycogen synthase kinase-3.[14] Notably, we are increasingly interested in using PET to understand mechanisms underlying the increased accumulation of amyloid in the central nervous system (CNS) in AD. This includes potential upregulation of mediators responsible for moving amyloid across the blood−brain barrier into the CNS (e.g., receptor for advanced glycation endproducts (RAGE)), as well as down regulation of transporters responsible for clearing

Received: December 4, 2015
Accepted: January 15, 2016
Published: January 15, 2016

DOI: 10.1021/acschemneuro.5b00319
ACS Chem. Neurosci. 2016, 7, 391−398

it back out again (e.g., P-glycoprotein (Pgp) and aquaporin-4). While there are PET radiotracers for Pgp[15] and aquaporin-4,[16] there are no small molecule radiotracers for quantifying CNS RAGE activity. Such a radiotracer could allow detection of AD prior to onset of amyloid accumulation and therefore, in an attempt to bolster the constellation of alternative AD imaging agents, we examined the feasibility of RAGE as a target for AD imaging using PET.

RAGE is a 35 kDa transmembrane receptor that belongs to the immunoglobulin superfamily of cell surface molecules. RAGE binds a variety of ligands[17] and is heavily implicated in AD[18] where it is thought to mediate the transport of peripheral Aβ across the BBB.[18] Though the exact mechanism of transport is unknown, it has been shown in cell assays that Aβ binding to RAGE initiates an inflammatory response and alters the tight junctions through the Ca^{2+}−calcineurin pathway.[19] Although in mice it has been suggested that the organic anion transporter polypeptide (Oatp1a4) is responsible for importing Aβ into the CNS, no comparable transporter has been identified in humans.[20] Therefore, this loss of BBB integrity may simply lead to an increase in the influx of Aβ into the brain. Moreover, RAGE-dependent signaling mediates downregulation of exporters of Aβ,[21] upregulation of β-secretase,[22] and neuroinflammatory responses,[23] and stimulates tau phosphorylation.[17] RAGE is upregulated and amplifies early Aβ neurotoxicity when Aβ levels are low.[24,25] Low doses of azeliragon (TTP-448), a RAGE antagonist, were associated with decreased cognitive decline relative to placebo in phase 2 clinical trials for mild to moderate AD.[26]

There are 22 documented isoforms of RAGE in humans, 12 of which are found in the brain.[27] These isoforms vary by alternative splicing, which includes a soluble form in addition to the cell membrane bound receptors. Aβ binds to the V domain of RAGE,[28] which is varied in the different isoforms. In AD, there is an overexpression of RAGE and a lower amount of the soluble splice variant sRAGEΔ, which is hypothesized to negatively regulate signal transduction of full length RAGE.[29] The relationship between RAGE and its various isoforms is not completely understood. PET radiotracers would aid in elucidating the complexity of this receptor and its dynamic relationship with Aβ in early stages of AD.

Prior efforts to produce radioligands for *in vivo* RAGE quantification have yielded a ^{99m}Tc monoclonal antibody[30] and ^{18}F labeled S100 protein.[31] While these probes have shown value for imaging outside of the central nervous system,[32,33] their preparation is relatively cumbersome and they are too large to efficiently cross the BBB. Because macromolecules are largely precluded from neuroimaging and because single photon emission computed tomography (SPECT) is of much lower sensitivity than PET,[34] this work commenced by investigating a promising small-molecule scaffold amenable to positron emitting isotopic labeling (ideally ^{11}C or ^{18}F).

A number of small-molecule mediators of RAGE interactions have been reported.[35−38] *N*-Benzyl-4-chloro-*N*-cyclohexylbenzamide (FPS-ZM1, Figure 1) is a multimodal RAGE-specific inhibitor that reduced amyloid-β-mediated brain dysfunction in a mouse model of AD. Despite having high lipophilicity (CLogP = 5.25; ChemBioDraw), FPS-ZM1 appeared to be a promising scaffold around which to develop a PET radiotracer because of its high affinity (25 nM K_i against RAGE−Aβ_{1-40}), BBB permeability,[37] lack of toxicity in mice or cells, reported specificity, and amenability to nucleophilic aromatic radiofluorination. Moreover, in a mouse model of AD with

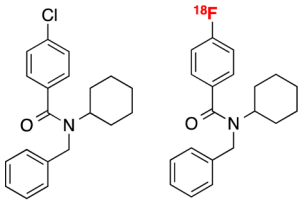

Figure 1. FPS-ZM1 and [^{18}F]RAGER.

confirmed Aβ pathology (aged *APP*$^{sw/0}$ mice overexpressing human Aβ), FPS-ZM1 was found to bind exclusively to RAGE, inhibiting RAGE-mediated influx of circulating Aβ into the CNS, reducing microglia activation and associated neuroinflammation.[37] In this work, we report the synthesis and preliminary preclinical evaluation of [^{18}F]RAGER: a PET probe based on FPS-ZM1 and the first BBB-penetrative small molecule radiotracer for RAGE.

RESULTS AND DISCUSSION

Chemistry. The first step when developing novel PET radiotracers is to synthesize both the precursor to be radiolabeled and the corresponding unlabeled reference standard to confirm identity of the radiolabeled product by HPLC. Unlabeled reference standard **2** was produced in good yield (80% over two steps) via a reductive amination of benzaldehyde and cyclohexylamine to give **1**, followed by acylation with 4-fluorobenzoyl chloride (Scheme 1). Trimethylammonium precursor **3** was prepared for radiolabeling as the charged precursor and uncharged product were expected to have markedly different retention times by reverse-phase HPLC. Precursor **3** was synthesized in the same manner as the reference standard, by acylation of intermediate **1** with *p*-(*N*,*N* dimethylamino)benzoyl chloride; subsequent alkylation with methyl iodide provided **3** in 10% yield (over three steps).

With precursor and reference standard in hand, we moved to radiolabeling. Radiosynthesis of [^{18}F]RAGER was automated using a commercial synthesis module (General Electric Tracerlab FX_{FN}) by reacting trimethylammonium precursor **3** with [^{18}F]fluoride in the presence of Kryptofix-2.2.2 (K2.2.2) in DMF at 130 °C for 30 min. Subsequent purification by semipreparative HPLC and reformulation yielded [^{18}F]RAGER (**4**) in satisfactory radiochemical yield (44 ± 10 mCi; 2.9% nondecay corrected based upon 1.5 Ci of [^{18}F]fluoride), excellent radiochemical purity (RCP) (>99%), and high specific activity (3740 ± 495 Ci/mmol); n = 6. Formulated [^{18}F]RAGER was stable for at least 60 min after the end of synthesis.

Preclinical Evalaution. *In Vitro Immunohistochemistry and Autoradiography.* Because imaging of RAGE is of interest in the context of Alzheimer's disease, tissue samples from an Alzheimer's patient were obtained, along with samples from a healthy control, to evaluate [^{18}F]RAGER. RAGE expression is known to be significantly elevated in the cortex,[39] and so cortical sections were selected from each subject for testing. Immunohistochemistry was performed with monoclonal anti-RAGE antibodies and HRP-conjugated secondary antibodies on each sample. For each AD patient, a 2.9-fold increase in RAGE expression was observed compared with normal control tissue (see Supporting Information for more details). This is

DOI: 10.1021/acschemneuro.5b00319
ACS Chem. Neurosci. 2016, 7, 391−398

Scheme 1. Radiosynthesis of HPLC Reference Standard (2), Precursor (3), and [^{18}F]RAGER (4)

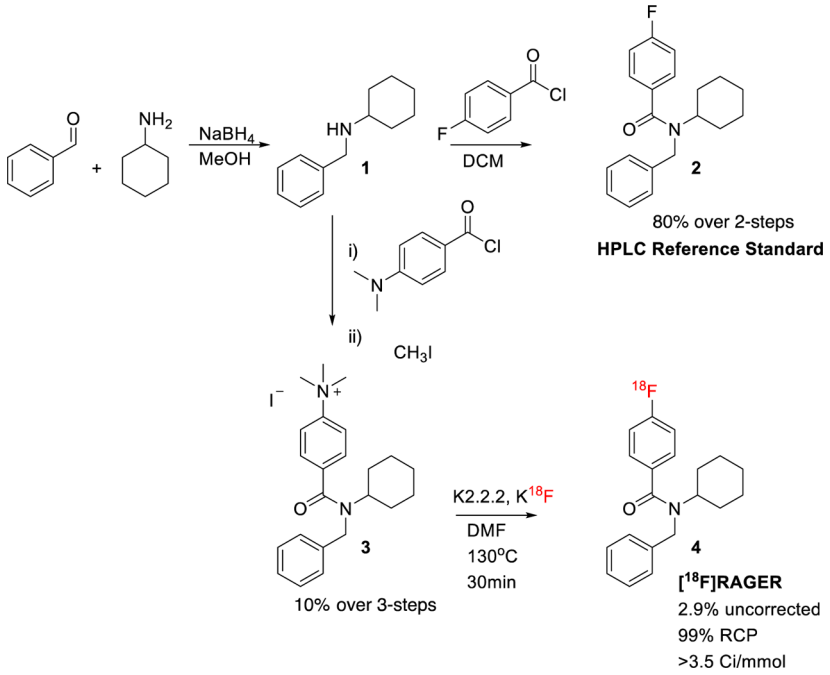

consistent with the known increased expression of RAGE in AD from the literature.

Adjacent sections were then incubated with [^{18}F]RAGER, **4** (Figure 2). The images confirm colocalization of [^{18}F]RAGER in gray matter areas with known RAGE expression, previously identified by immunohistochemistry. There was higher uptake in the AD samples than the normal control samples. Nonspecific binding was investigated by repeating incubations in the presence of 1000-fold excess of unlabeled RAGER, which confirmed that binding in the gray matter regions was displaceable to background levels. However, despite the reported specificity of the parent compound,[37] we did observe significant nonspecific binding in the white matter (the white matter signal in the nonspecific binding experiments shown in Figure 2 actually appears higher than that for the total binding experiments. The cause of this is unclear, but it is possible that all of the displaced radiotracer in the nonspecific samples gets retained in the white matter leading to the higher signal). Although RAGER has lower lipophilicity (experimental log P = 3.5; CLogP = 4.85, ChemBioDraw) than FPS-ZM1 (CLogP = 5.25, ChemBioDraw), it is still lipophilic, and we believe this is the origin of the high white matter binding. Correcting for nonspecific binding allowed estimation of K_d and B_{max} in both the AD tissue and normal control tissue (Table 1). Using both AD and control tissue samples, the K_d was found to be approximately 15 nM, similar to the reported K_i of 25 nM for FPS-ZM1.[37] The B_{max} in AD tissue was found to be 2.8-fold higher than the B_{max} in normal control tissue, which is also consistent with the 2.9-fold increase in RAGE expression confirmed by immunohistochemistry (*vide supra*). The binding potential (BP), estimated by the B_{max}/K_d value, is useful for predicting the suitability of a radiotracer for imaging a target binding site in human subjects. [^{18}F]RAGER has a BP of 1.86 in AD tissue, suggesting potential suitability of this scaffold for future applications in clinical PET imaging and the feasibility of imaging RAGE with PET.

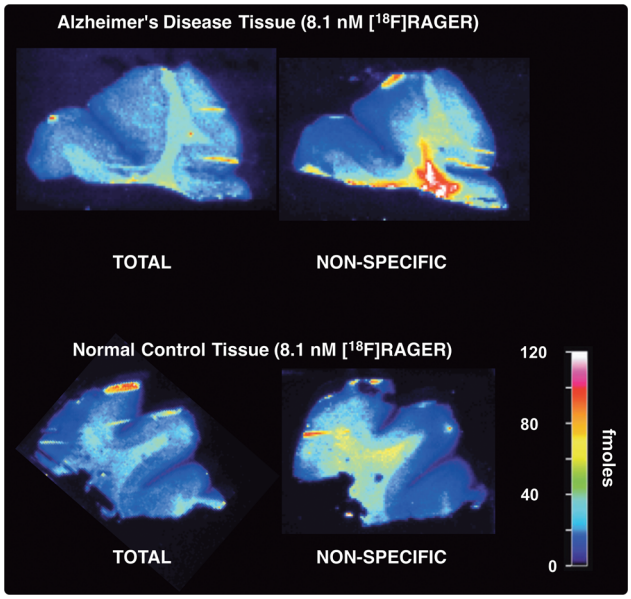

Figure 2. Autoradiographic images of [^{18}F]RAGER in AD and normal control frontal cortex samples.

Table 1. Binding Affinity Data for [^{18}F]RAGER

	K_d (nM)	B_{max} (nM)	BP (B_{max}/K_d)
AD tissue	15.5	28	1.86
normal control tissue	15.3	10	0.65

Docking Studies. Docking studies were performed with Autodock Vina[40] using a 1.5 Å resolution crystal structure (PDB 3O3U[41]) to generate a feasible binding mode of the RAGER−RAGE complex (Figure 3; see Supporting Information for further details). Because there is no known crystal structure of any small molecule RAGE antagonists with RAGE, Vina's search space was defined to encompass the interface residues for the vRAGE−S100P interaction as determined by

DOI: 10.1021/acschemneuro.5b00319
ACS Chem. Neurosci. 2016, 7, 391−398

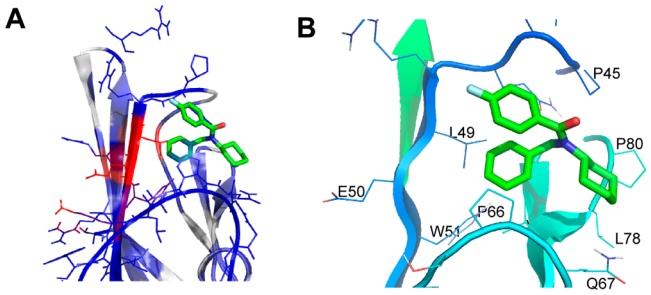

Figure 3. Possible configuration of RAGER bound to vRAGE. (A) The blue color indicates interface residues of RAGE-S100P, and the bright red is β-strand important for the RAGE−Aβ interaction.[28] (B) Close up of possible binding with labeled residues.

the NMR-solved complex (PDB 2MJW).[42] Yu et al. found FPS-ZM1 to be an inhibitor of the RAGE−S100P mediated cell proliferation induction,[43] and we reasoned, because of its structural similarities to FPS-ZM1, that RAGER would bind in the same pocket. This assumption is supported by similar binding energies calculated for the lowest energy conformations of RAGER (−6.6 kcal/mol) and FPS-ZM1 (−6.5 kcal/mol). This, in combination with the apparent interaction of the ligands with conserved residues (L49, W51) of the β3 strand, previously shown to be important for the RAGE−Aβ interaction,[28] suggests that it is a reasonable docking configuration. The interaction appears to be largely dependent on hydrophobic interactions, although high-resolution structural information on a RAGE−inhibitor complex is needed to definitely confirm the binding mechanism of the scaffold. Nevertheless, these *in silico* studies do support our supposition that the chlorine/fluorine substitution of RAGER in relation to FPS-ZM1 had little effect on best bound-ligand conformation or energy.

Preclinical Imaging. *In vivo* behavior of the radiotracers was investigated initially in rodents (n = 3). PET scans were conducted in Sprague−Dawley rats, and imaging was conducted for 90 min postinjection of the radiotracer. Following the scan, images were summed (Figure 4a) and a region-of-interest (ROI) was drawn over the whole brain on multiple planes. The volumetric ROIs were then applied to the full dynamic data set to generate a time−radioactivity curve (Figure 4b). The curve showed rapid uptake of [^{18}F]RAGER (peak SUV ≈ 2.5). Peak uptake occurred within 3 min postinjection and was followed by virtually complete washout over the duration of the PET scan. Encouraged by these results, we also evaluated the imaging properties of [^{18}F]RAGER in non-human primates. Similar imaging results were obtained in rhesus macaque (Figure 4c). A ROI was drawn initially for the whole brain and used to generate a time−radioactivity curve (Figure 4d), which revealed rapid uptake of [^{18}F]RAGER in the primate brain (peak SUV ≈ 2.3). Peak uptake again occurred within 3 min postinjection, and was followed by washout over the duration of the PET scan. Washout was faster in rodents

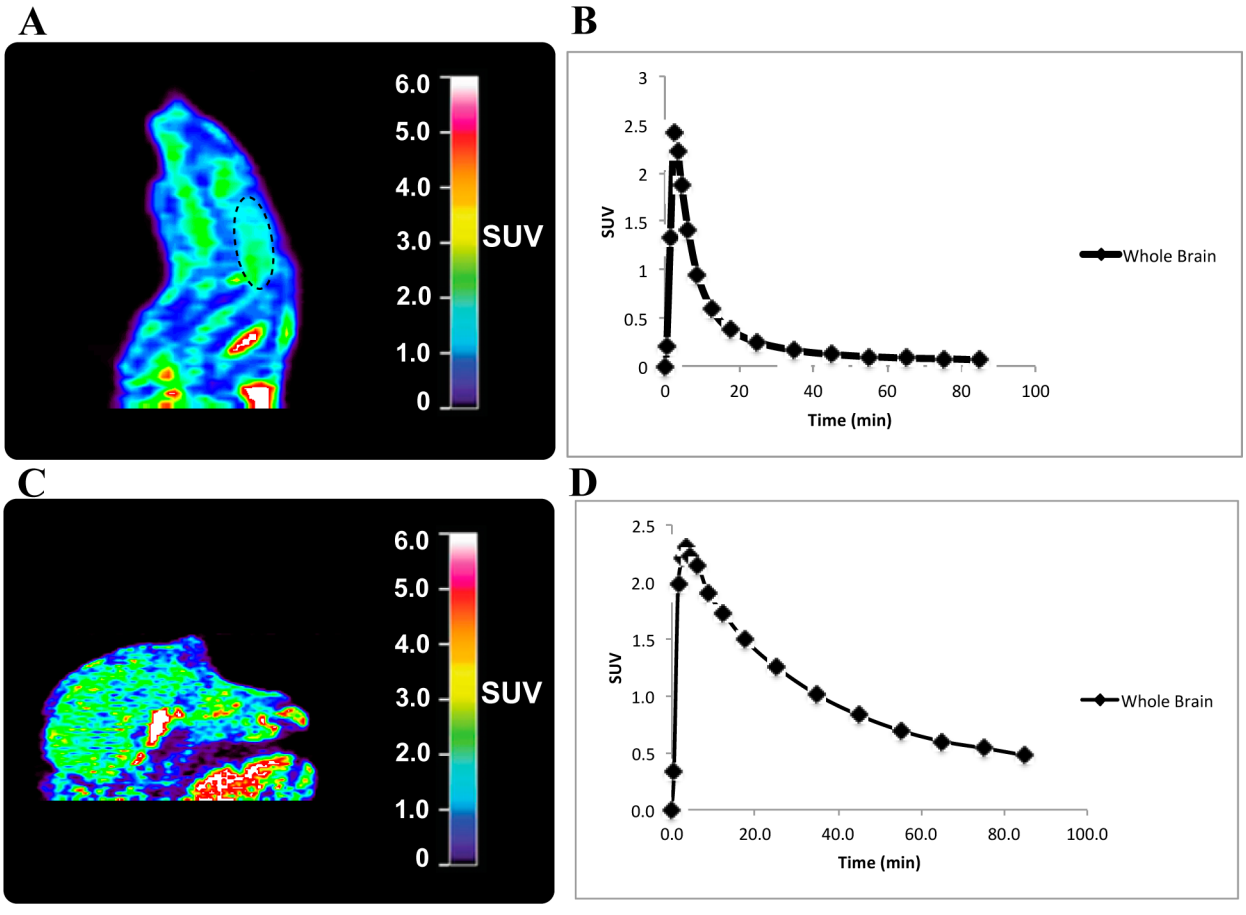

Figure 4. Representative microPET imaging data for rodent (A, summed images 0−90 min post-iv-injection of the radiotracer (dotted oval = brain); B, rodent whole brain time−radioactivity curves) and non-human primate (C, summed images 0−90 min post-iv-injection of the radiotracer; D, non-human primate whole brain time−radioactivity curves) imaged with [^{18}F]RAGER.

DOI: 10.1021/acschemneuro.5b00319
ACS Chem. Neurosci. 2016, 7, 391−398

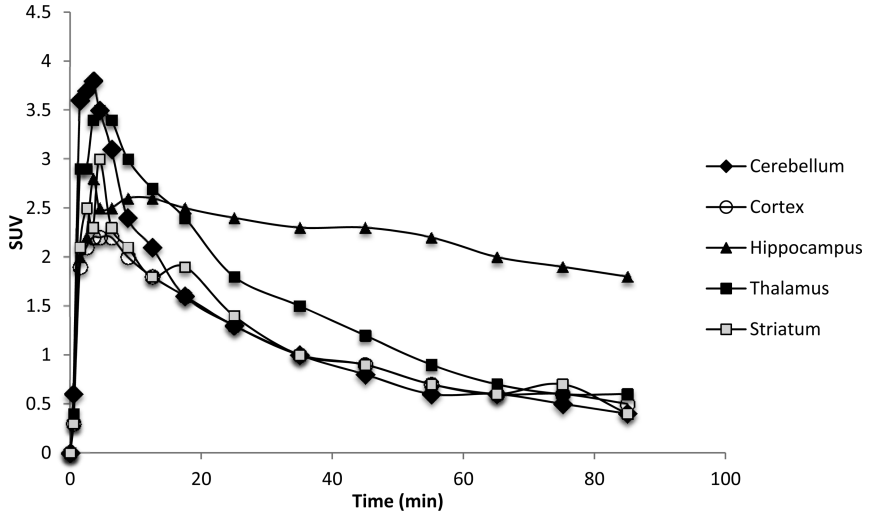

Figure 5. [^{18}F]RAGER regional time−radioactivity curves in the non-human primate brain.

than primates, and we attribute this to increased tissue volumes and lower blood flow in the primates. The radiotracer provided reasonable levels of uptake in all gray matter regions (peak SUVs range from 2−4; see Figure 5 for regional time−radioactivity curves of [^{18}F]RAGER in non-human primate brain). For example, there was high uptake apparent in the cortex and cerebellum, which agrees with the reported distribution of RAGE.[39] Notably, there was also extensive bilateral uptake and markedly slower washout associated with the hippocampal regions, which suggests specific binding. This is also consistent with the known expression of RAGE, where it has been shown that some RAGE expression is normal in the healthy hippocampus but that elevated levels are present in the hippocampus of the Alzheimer's disease brain.[39b−e] Very little white matter binding was apparent, in contrast to the high degrees of nonspecific binding that complicated the *in vitro* studies described above, although there was extensive uptake in the brain stem and an unknown region outside of the brain (possibly tissue associated with the nasal cavity). The cause of differing nonspecific binding between the *in vitro* and *in vivo* studies could simply be that there is less [^{18}F]RAGER available to bind in the brain during the *in vivo* studies because of uptake in the periphery (there is high RAGE expression in the lung[44]), binding to circulating soluble RAGE or could be due to metabolism effects. To investigate the latter possibility, we next investigated metabolism of RAGER.

Metabolism. Metabolism of RAGER was examined by incubation with rat liver microsomes (see Supporting Information). The LC-MS/MS data analysis at microsome incubation time points out to 60 min demonstrated extremely fast metabolism of the radiotracer, with a half-life of 0.66 min and only ∼0.5% of authentic RAGER remaining at 5 min. Although we have not confirmed this metabolism profile *in vivo*, the rodent time−radioactivity curves are consistent with rapid metabolism and do not suggest that any labeled metabolites enter the brain. Rapid metabolism would explain the difference between the high nonspecific binding observed *in vitro* and the low levels apparent in the PET images. We have also not examined metabolism in primates but would expect it to be slower than that in rats. This could lead to higher nonspecific binding in primates, which would be consistent with the slower washout apparent in the primate time−radioactivity curves (Figure 4). The rapid metabolism also suggests that brain uptake in known areas of RAGE expression is likely occurring before first pass metabolism, which is again consistent with the rapid peak uptake of the radiotracer in both rats and primates.

SUMMARY AND FUTURE OUTLOOK

In summary, we have demonstrated the synthesis and preliminary preclinical evaluation of [^{18}F]RAGER: the first small molecule BBB-permeable PET radioligand for the receptor for advanced glycation end-products. We have confirmed upregulation of RAGE in AD post-mortem cortical tissue with immunohistochemistry and demonstrated that [^{18}F]RAGER colocalizes with areas of RAGE distribution. Using molecular docking, we identified a reasonable binding site for RAGER. MicroPET imaging in rodent and non-human primate confirmed brain uptake and extensive washout, and the latter indicated that the radiotracer accumulates in areas of known RAGE expression.

The binding potential (BP), estimated by the B_{max}/K_d value, is useful for predicting the suitability of a radiotracer for imaging a target binding site in human subjects. While the ideal binding potential is unknown, useful radiotracers have a binding potential that falls within a range of values, although ≥5 has recently been recommended for CNS radiotracers by the National Institutes of Health. [^{18}F]RAGER has a BP of 1.86 in AD tissue, suggesting potential suitability of this scaffold for future applications in clinical PET imaging of RAGE but leaving scope for improvement. Second generation radiotracers with K_d ≤ 6 nM are desirable to achieve the target BP of ≥5 for anticipated successful *in vivo* clinical imaging of RAGE in the future. To address this, efforts to develop new radioligands based around the FPS-ZM1 scaffold that improve affinity, reduce lipophilicity to minimize nonspecific binding, and address rapid metabolism of the tracer are ongoing and will be the subject of a future report. We expect PET radiotracers for RAGE to be useful in AD as well as other diseases in which dysfunction of RAGE has been implicated in such as cancer, diabetes, and atherosclerosis.[45,46]

EXPERIMENTAL SECTION

Chemistry. *General Considerations.* All the chemicals employed in the syntheses were sourced commercially and used without further purification. ^{1}H NMR spectra were obtained at 400 MHz on Varian NMR spectrometer in CD_3OD or d_6-DMSO solutions at room

DOI: 10.1021/acschemneuro.5b00319
ACS Chem. Neurosci. 2016, 7, 391−398

temperature with tetramethylsilane (TMS, δ = 0) as an internal standard. ^{13}C NMR spectra were obtained at 100 MHz, and ^{19}F-NMR spectra were obtained at 376 MHz. Chemical shifts (δ) are reported in ppm, and coupling constants are reported in hertz. Multiplicity is defined by s (singlet), d (doublet), t (triplet), q (quartet), and m (multiplet). High performance liquid chromatography (HPLC) was performed using a Shimadzu LC-2010A HT system equipped with a Bioscan B-FC-1000 radiation detector. Mass spectra were performed on a Micromass VG 70-250-S magnetic sector mass spectrometer, Micromass AutoSpec Ultima magnetic sector mass spectrometer, or Agilent Q-TOF HPLC-MS using the electrospray ionization (ESI) method or electron ionization (EI) method.

*Preparation of N-Benzyl-N-cyclohexyl-4-fluorobenzamide (**2**).* Cyclohexylamine (250 mg, 2.52 mmol) and benzaldehyde (267 mg, 2.52 mmol) were dissolved in methanol (5 mL). Sodium sulfate was added, and the mixture was stirred for 18 h at 50 °C. The mixture was filtered, and the filtrate was concentrated *in vacuo*. The white semisolid was redissolved in methanol and cooled to 0 °C. Sodium borohydride (133 mg, 3.53 mmol) was slowly added, and the reaction was stirred at rt for 4 h. The reaction was quenched with saturated ammonium chloride solution. The intermediate product was extracted with dichloromethane (3×) and dried over sodium sulfate, and solvent was removed *in vacuo*. The intermediate product was dissolved in dichloromethane (6 mL), and the solution was cooled to 0 °C. Triethylamine (306 mg, 3.02 mmol) and 4-fluorobenzoyl chloride (439 mg, 2.77 mmol) were added, and the solution was stirred for 18 h under argon. The reaction was quenched with H_2O, and the product was extracted with dichloromethane (3×) and purified by flash chromatography (SiO_2, 3:1 = hexanes/ethyl acetate). This process yielded the product as white, crystalline solid (628 mg, 80%); R_f = 0.52 (SiO_2, 3:1 = hexanes/ethyl acetate); ^{1}H NMR (400 MHz; DMSO-d_6)/δ (ppm) 0.97−1.63 (10H, m), 3.48 (1H, br), 4.63 (2H, s), 7.21−7.51 (9H, m); ^{13}C NMR (100 MHz; DMSO-d_6)/δ (ppm) 25.03, 25.80, 31.45, 51.17, 59.20, 115.98, 126.85, 127.08, 128.76, 129.06, 134.14, 139.96, 163.84, 170.61; ^{19}F NMR (376.3 MHz, DMSO-d_6)/δ (ppm) −111.71(1F, s); HPLC: 98%, retention time =22 min, column Phenomenex Gemini C18, 250 mm × 4.6 mm, mobile phase 10 mM NH_4HCO_3 in 58% MeCN, plus 2 mL/L sat. NH_4OH solution, flow rate = 1.0 mL/min, wavelength = 254 nm; HRMS calculated for $[M + H]^+$ (M = $C_{20}H_{22}FNO$) 312.1758, found 312.1756.

*Preparation of 4-(Benzyl(cyclohexyl)carbamoyl)-N,N,N-trimethylbenzenaminium Iodide (**3**).* To a vial was added *N*-benzyl-*N*-cyclohexyl-4-(dimethylamino)benzamide (35.0 mg, 0.104 mmol, see Supporting Information for synthesis procedure) and methyl iodide (60.7 mg, 0.428 mmol). The vial was sealed, heated to 45 °C, and stirred. Additional methyl iodide (60.7 mg, 0.428 mmol, 20 times) was added over a few hours. After 5 h, an off-white, insoluble semisolid was observed. After 12 h, the solvent was evaporated under vacuum. The solid residue was washed with hexanes (3 × 2 mL) and diethyl ether (1 × 2 mL) and dried under vacuum to yield the product as an off-white solid (35.6 mg, 0.0744 mmol, 72%); R_f = 0.53 (SiO_2, 3:1 = dichloromethane/methanol); ^{1}H NMR (400 MHz; CD_3OD, 55 °C)/δ (ppm) 1.09(3H, m), 1.59−1.73(7H, m), 3.70 (9H, s), 4.67(2H, s), 7.22−7.30(5, m), 7.66(2H, s), 7.98(2H, s); HRMS calculated for $[M]^+$ (M = $C_{23}H_{31}N_2O$) 351.2431, found 351.2429.

Radiochemistry. *General Considerations.* Unless otherwise stated, reagents and solvents were commercially available and used without further purification: sodium chloride, 0.9% USP, and sterile water for injection, USP, were purchased from Hospira; ethanol was purchased from American Regent; HPLC grade acetonitrile was purchased from Fisher Scientific. Other synthesis components were obtained as follows: sterile filters were obtained from Millipore; sterile product vials were purchased from Hollister-Stier; QMA-light and C18-light Sep-Paks were purchased from Waters Corporation. Sep-Paks were flushed with 10 mL of ethanol followed by 10 mL of sterile water prior to use.

*[^{18}F]RAGER (**4**).* [^{18}F]KF was prepared using a TRACERLab FX_{FN} automated radiochemistry synthesis module (General Electric, GE). [^{18}F]Fluoride was produced via the ^{18}O(p,n)^{18}F nuclear reaction using a 16 MeV GE PETTrace cyclotron (40 μA beam for 30 min generated 1500 mCi of [^{18}F]fluoride). The [^{18}F]fluoride was delivered to the synthesis module (in a 1.5 mL bolus of [^{18}O]water) and trapped on a QMA-light Sep-Pak to remove [^{18}O]water. [^{18}F]Fluoride was eluted into the reaction vessel using K_2CO_3 (3.5 mg in 0.5 mL of water). A solution of K2.2.2 (15 mg in 1 mL of acetonitrile) was added to the reaction vessel, and the resulting solution was azeotropically dried by heating the reaction vessel to 100 °C and drawing vacuum for 4 min. After this time, the reaction vessel was subjected to an argon stream and simultaneous vacuum draw for an additional 4 min. RAGER precursor **3** (1.5 mg dissolved in 0.5 mL of DMF) was delivered to the reaction vessel, and the reaction was heated to 130 °C and stirred for 30 min. After this time, the reactor was cooled to 55 °C and 2 mL of semipreparative HPLC solvent was added to the crude reaction mixture. This mixture was injected onto a semipreparative HPLC column (column Phenomenex Gemini C18, 250 mm × 10 mm; mobile phase 10 mM NH_4HCO_3 in 58% MeCN, pH 9.0 adjusted with 2 mL/L sat. NH_4OH, flow rate = 2.5 mL/min; see Supporting Information Figure S1 for a representative HPLC trace). The product peak (∼36−37 min retention time) was collected and diluted into a round-bottom flask containing 50 mL of water. The solution was then passed through a C-18 extraction disk to remove organic solvent. The disk was washed with 5 mL of sterile water. The product was eluted with 0.5 mL of ethanol followed by 4.5 mL of normal saline. The final formulation was passed through a 0.2 μM needle filter into a sterile dose vial. Using Nitro-precursor, we obtained 15.3 ± 6.4 mCi (566 ± 237 MBq), 1.0% uncorrected yield, >99% RCP, pH = 5−5.5, n = 4. Using trimethylammonium precursor, we obtained 44.6 ± 10 mCi (1650 ± 385 MBq), 3.0% uncorrected yield, > 99% RCP, 3740 ± 495 Ci/mmol (138 ± 18 GBq/mmol), pH = 5.5, n = 6.

Quality Control. Quality control of radiopharmaceutical doses was conducted using the following tests.

Visual Inspection. Doses were examined visually to confirm that they were clear, colorless, and free of particulate matter.

Dose pH. The pH of the doses was analyzed by applying a small amount of the dose to pH-indicator strips and determined by visual comparison with the provided scale.

HPLC Analysis. Radiochemical purity of [^{18}F]RAGER was assessed using Shimadzu LC-2010A HT system equipped with the UV and Rad detectors (column Phenomenex Gemini C18, 250 mm × 4.6 mm; mobile phase 10 mM NH_4HCO_3 in 58% MeCN, pH 9 adjusted with 2 mL/L sat. NH_4OH solution; flow rate = 1.0 mL/min; wavelength = 254 nm; room temperature; product peak ≈ 22.5 min; see Supporting Information Figure S2 for a representative HPLC trace).

■ ASSOCIATED CONTENT

Ⓢ Supporting Information

The Supporting Information is available free of charge on the ACS Publications website at DOI: 10.1021/acschemneuro.5b00319.

Experimental procedures and spectra for all novel compounds synthesized and procedures for binding affinity experiments, docking experiments, microPET imaging, liver microsome metabolism studies, log *P* determination, autoradiography, and immunohistochemistry (PDF)

■ AUTHOR INFORMATION

Corresponding Author

*Prof. Peter J. H. Scott. Tel: +1(734)615-1756. Fax: +1(734) 615-2557. E-mail: pjhscott@umich.edu.

Author Contributions

The manuscript was written through contributions of all authors. All authors have given approval to the final version of the manuscript.

DOI: 10.1021/acschemneuro.5b00319
ACS Chem. Neurosci. 2016, 7, 391−398

Funding

Financial support of this work from the National Institutes of Health (Grants T32-GM007767 and T32-EB005172) is gratefully acknowledged. The content of this article is solely the responsibility of the authors and does not necessarily represent the official views of the National Institutes of Health. Additional funding for this research from the Alzheimer's Association (Grant NIRP-14-305669), and the University of Michigan (College of Pharmacy and Undergraduate Research Opportunity Program) is gratefully acknowledged. The Michigan Alzheimer's Disease Center is funded by the National Institute of Aging (Grant P50-AG08671) as well as a gift from an anonymous donor.

Notes

The authors declare no competing financial interest.

■ ACKNOWLEDGMENTS

The authors thank the Michigan Alzheimer's Disease Center Brain Bank for selecting and providing brain samples.

■ ABBREVIATIONS

Aβ, amyloid β; AD, Alzheimer's disease; BBB, blood−brain barrier; CNS, central nervous system; HPLC, high-performance liquid chromatography; IPA, isopropanol; K2.2.2, Kryptofix-2.2.2; MAP, maximum a posteriori; MS, mass spectrometry; NMR, nuclear magnetic resonance; PET, positron emission tomography; Pgp, P-glycoprotein transporter; PiB, Pittsburgh compound B; QMA, quaternary methylammonium; RAGE, receptor for advanced glycation endproducts; RCP, radiochemical purity; RCY, radiochemical yield; ROI, region-of-interest; SA, specific activity; TACs, time−radioactivity curves

■ REFERENCES

(1) Klunk, W. E., Engler, H., Nordberg, A., Wang, Y., Blomqvist, G., Holt, D. P., Bergström, M., Savitcheva, I., Huang, G.-F., Estrada, S., Ausén, B., Debnath, M. L., Barletta, J., Price, J. C., Sandell, J., Lopresti, B. J., Wall, A., Koivisto, P., Antoni, G., Mathis, C. A., and Långström, B. (2004) Imaging brain amyloid in Alzheimer's disease with Pittsburgh Compound-B. *Ann. Neurol. 55*, 306−319.

(2) Wong, D. F., Rosenberg, P. B., Zhou, Y., Kumar, A., Raymont, V., Ravert, H. T., Dannals, R. F., Nandi, A., Brašić, J. R., Ye, W., Hilton, J., Lyketsos, C., Kung, H. F., Joshi, A. D., Skovronsky, D. M., and Pontecorvo, M. J. (2010) In vivo imaging of amyloid deposition in Alzheimer disease using the radioligand ^{18}F-AV-45 (Flobetapir F18). *J. Nucl. Med. 51*, 913−920.

(3) Chételat, G., La Joie, R., Villain, N., Perrotin, A., de La Sayette, V., Eustache, F., and Vandenberghe, R. (2013) Amyloid Imaging in Cognitively Normal Individuals, at-Risk Populations and Preclinical Alzheimer's Disease. *NeuroImage: Clin. 2*, 356−365.

(4) (a) Villemagne, V. L., Fodero-Tavoletti, M. T., Masters, C. L., and Rowe, C. C. (2015) Tau imaging: early progress and future directions. *Lancet Neurol. 14*, 114−124. (b) Ariza, M., Kolb, H. C., Moechars, D., Rombouts, F., and Andrés, J. I. (2015) Tau positron emission tomography (PET) imaging: past, present, and future. *J. Med. Chem. 58*, 4365−4382.

(5) Kepe, V., Moghbel, M. C., Langstrom, B., Zaidi, H., Vinters, H. V., Huang, S.-C., Satyamurthy, N., Doudet, D., Mishani, E., Cohen, R. M., Hoilund-Carlsen, P. F., Alavi, A., and Barrio, J. R. (2013) Amyloid-β Positron Emission Tomography Imaging Probes: A Critical Review. *J. Alzheimer's Dis. 36*, 613−631.

(6) Moreth, J., Mavoungou, C., and Schindowski, K. (2013) Is abeta a sufficient biomarker for monitoring anti-abeta clinical studies? A critical review. *Front. Aging Neurosci. 5*, No. 25.

(7) Plassman, B. L., Langa, K. M., Fisher, G. G., Heeringa, S. G., Weir, D. R., Ofstedal, M. B., Burke, J. R., Hurd, M. D., Potter, G. G., Rodgers, W. L., Steffens, D. C., Willis, R. J., and Wallace, R. B. (2007) Prevalence of dementia in the United States: the aging, demographics, and memory study. *Neuroepidemiology 29*, 125−132.

(8) Duthey, B. (2013) *Update on 2004 Background Paper Alzheimer Disease and Other Demntias. Priority Medicines for Europe and the World; A Public Health Approach to Innovation*, WHO, Geneva, Switzerland.

(9) Holland, J. P., Liang, S. H., Rotstein, B. H., Collier, T. L., Stephenson, N. A., Greguric, I., and Vasdev, N. (2014) Alternative approaches for PET radiotracer development in Alzheimer's disease: imaging beyond plaque. *J. Labelled Compd. Radiopharm. 57*, 323−331.

(10) Mach, R. H. (2014) New targets for the development of PET tracers for imaging neurodegeneration in Alzheimer disease. *J. Nucl. Med. 55*, 1221−1224.

(11) Cary, B. P., Brooks, A. F., Fawaz, M. V., Shao, X., Desmond, T. J., Carpenter, G. M., Sherman, P., Quesada, C. A., Albin, R. L., and Scott, P. J. H. (2015) Targeting metal-Aβ aggregates with bifunctional radioligand [^{11}C]L2-b and a fluorine-18 analogue [^{18}F]FL2-b. *ACS Med. Chem. Lett. 6*, 112−116.

(12) Liang, S. H., Holland, J. P., Stephenson, N. A., Kassenbrock, A., Rotstein, B. H., Daignault, C. P., Lewis, R., Collier, L., Hooker, J. M., and Vasdev, N. (2015) PET neuroimaging studies of [^{18}F]CABS13 in a double transgenic mouse model of Alzheimer's disease and nonhuman primates. *ACS Chem. Neurosci. 6*, 535−541.

(13) Brooks, A. F., Jackson, I. M., Shao, X., Kropog, G. W., Sherman, P., Quesada, C. A., and Scott, P. J. H. (2015) Synthesis and evaluation of [^{11}C]PBD150, a radiolabeled glutaminyl cyclase inhibitor for the potential detection of Alzheimer's disease prior to amyloid β aggregation. *MedChemComm 6*, 1065−1068.

(14) (a) Cole, E. L., Shao, X., Sherman, P., Quesada, C., Fawaz, M. V., Desmond, T. J., and Scott, P. J. H. (2014) Synthesis and evaluation of [11C]PyrATP-1, a novel radiotracer for PET imaging of glycogen synthase kinase-3β (GSK-3β). *Nucl. Med. Biol. 41*, 507−512. (b) Li, L., Shao, X., Ohnmacht, S. A., Ferrari, V., Hong, Y. T., Williamson, D. J., Fryer, T. D., Quesada, C. A., Sherman, P., Riss, P. J., Scott, P. J. H., Aigbirhio, F. I., and Cole, E. L. (2015) Synthesis and initial in vivo studies with [^{11}C]SB-216763: the first radiolabeled brain penetrative inhibitor of GSK-3. *ACS Med. Chem. Lett. 6*, 548−552.

(15) Syvänen, S., and Eriksson, J. (2013) Advances in PET imaging of P-glycoprotein functiona at the blood-brain barrier. *ACS Chem. Neurosci. 4*, 225−237.

(16) Suzuki, Y., Nakamura, Y., Yamada, K., Huber, V. J., Tsujita, M., and Nakada, T. (2013) Aquaporin-4 positron emission tomography imaging of the human brain: first report. *J. Neuroimaging 23*, 219−223.

(17) Xie, J., Méndez, J. D., Méndez-Valenzuela, V., and Aguilar-Hernández, M. M. (2013) Cellular signalling of the receptor for advanced glycation end products (RAGE). *Cell. Signalling 25*, 2185−2197.

(18) Deane, R., Du, Y. S., Submamaryan, R. K., LaRue, B., Jovanovic, S., Hogg, E., Welch, D., Manness, L., Lin, C., Yu, J., Zhu, H., Ghiso, J., Frangione, B., Stern, A., Schmidt, A. M., Armstrong, D. L., Arnold, B., Liliensiek, B., Nawroth, P., Hofman, F., Kindy, M., Stern, D., and Zlokovic, B. (2003) RAGE mediates amyloid-beta peptide transport across the blood-brain barrier and accumulation in brain. *Nat. Med. 9*, 907−913.

(19) Kook, S.-Y., Hong, H. S., Moon, M., Ha, C. M., Chang, S., and Mook-Jung, I. (2012) Aβ_{1-42}-RAGE interaction disrupts tight junctions of the blood−brain barrier via Ca^{2+}-calcineurin signaling. *J. Neurosci. 32*, 8845−8854.

(20) Do, T. M., Bedussi, B., Chasseigneaux, S., Dodacki, A., Yapo, C., Chacun, H., Scherrmann, J. M., Farinotti, R., and Bourasset, F. (2013) Oatp1a4 and an L-thyroxine-sensitive transporter mediate the mouse blood-brain barrier transport of amyloid-β peptide. *J. Alzheimer's Dis. 36*, 555−561.

(21) Park, R., Kook, S.-Y., Park, J.-C., and Mook-Jung, I. (2014) Aβ_{1-42} reduces P-glycoprotein in the blood−brain barrier through RAGE−NF-κB signaling. *Cell Death Dis. 5*, e1299.

(22) Cho, H. J., Son, S. M., Jin, S. M., Hong, H. S., Shin, D. H., Kim, S. J., Huh, K., and Mook-Jung, I. (2009) RAGE regulates BACE1 and

DOI: 10.1021/acschemneuro.5b00319
ACS Chem. Neurosci. 2016, 7, 391−398

A generation via NFAT1 activation in Alzheimer's disease animal model. *FASEB J. 23*, 2639−2649.
(23) Fang, F., Lue, L. F., Yan, S., Xu, H., Luddy, J. S., Chen, D., Walker, D. G., Stern, D. M., Yan, S., Schmidt, A. M., Chen, J. X., and Yan, S. S. (2010) RAGE-dependent signaling in microglia contributes to neuroinflammation, Abeta accumulation, and impaired learning/memory in a mouse model of Alzheimer's disease. *FASEB J. 24*, 1043−1055.
(24) Perrone, L., Sbai, O., Nawroth, P., and Bierhaus, A. (2012) The Complexity of Sporadic Alzheimer's Disease Pathogenesis: The Role of RAGE as Therapeutic Target to Promote Neuroprotection by Inhibiting Neurovascular Dysfunction. *Int. J. Alzheimer's Dis.*, No. 734956.
(25) Cuevas, E., Lantz, S. M., Tobón-Velasco, J. C., Newport, G. D., Wu, Q., Virmani, A., Ali, S. F., and Santamaría, A. (2011) On the in vivo early toxic properties of Aβ25−35 peptide in the rat hippocampus: Involvement of the Receptor-for-Advanced Glycation-End-Products and changes in gene expression. *Neurotoxicol. Teratol. 33*, 288−296.
(26) Burstein, A. H., Grimes, I., Galasko, D. R., Aisen, P. S., Sabbagh, M., and Mjalli, A. M. (2014) Effect of TTP488 in patients with mild to moderate Alzheimer's disease. *BMC Neurol. 14*, No. 12.
(27) López-Díez, R., Rastrojo, A., Villate, O., and Aguado, B. (2013) Complex tissue-specific patterns and distribution of multiple RAGE splice variants in different mammals. *Genome Biol. Evol. 5*, 2420−2435.
(28) Kim, S.-J., Ahn, J.-W., Kim, H., Ha, H.-J., Lee, S.-W., Kim, H.-K., Lee, S., Hong, H.-S., Kim, Y. H., and Choi, C. Y. (2013) Two β-strands of RAGE participate in the recognition and transport of amyloid-β peptide across the blood brain barrier. *Biochem. Biophys. Res. Commun. 439*, 252−257.
(29) Zhu, H., and Ding, Q. (2015) Lower expression level of two RAGE alternative splicing isoforms in Alzheimer's disease. *Neurosci. Lett. 597*, 66−70.
(30) Tekabe, Y., Luma, J., Einstein, A. J., Sedlar, M., Li, Q., Schmidt, A. M., and Johnson, L. L. (2010) A novel monoclonal antibody for RAGE-directed imaging identifies accelerated atherosclerosis in diabetes. *J. Nucl. Med. 51*, 92−97.
(31) Wolf, S., Haase-Kohn, C., Lenk, J., Hoppmann, S., Bergmann, R., Steinbach, J., and Pietzsch, J. (2011) Expression, purification and fluorine-18 radiolabeling of recombinant S100A4: a potential probe for molecular imaging of receptor for advanced glycation endproducts in vivo? *Amino Acids 41*, 809−820.
(32) Tekabe, Y., Kollaros, M., Li, C., Zhang, G., Schmidt, A. M., and Johnson, L. (2013) Imaging receptor for advanced glycation end product expression in mouse model of hind limb ischemia. *EJNMMI Res. 3*, No. 37.
(33) Tekabe, Y., Kollaros, M., Li, Q., Zhang, G., Li, C., Schmidt, A. M., and Johnson, L. L. (2014) Beneficial effect of glucose control on atherosclerosis progression in diabetic ApoE $^{-/-}$ mice: shown by RAGE directed imaging. *Int. J. Mol. Imaging 2014*, No. 695391.
(34) Rahmim, A., and Zaidi, H. (2008) PET versus SPECT: strengths, limitations and challenges. *Nucl. Med. Commun. 29*, 193−207.
(35) Han, Y. T., Choi, G.-I., Son, D., Kim, N.-J., Yun, H., Lee, S., Chang, D. J., Hong, H.-S., Kim, H., Ha, H.-J., Kim, Y.-H., Park, H.-J., Lee, J., and Suh, Y.-G. (2012) Ligand-based design, synthesis, and biological evaluation of 2-aminopyrimidines, a novel series of receptor for advanced glycation end products (RAGE) inhibitors. *J. Med. Chem. 55*, 9120−9135.
(36) Han, Y. T., Kim, K., Choi, G.-I., An, H., Son, D., Kim, H., Ha, H.-J., Son, J.-H., Chung, S.-J., Park, H.-J., Lee, J., and Suh, Y.-G. (2014) Pyrazole-5-carboxamides, novel inhibitors of receptor for advanced glycation end products (RAGE). *Eur. J. Med. Chem. 79*, 128−142.
(37) Deane, R., Singh, I., Sagare, A. P., Bell, R. D., Ross, N. T., LaRue, B., Love, R., Perry, S., Paquette, N., Deane, R. J., Thiyagarajan, M., Zarcone, T., Fritz, G., Friedman, A. E., Miller, B. L., and Zlokovic, B. V. (2012) A multimodal RAGE-specific inhibitor reduces amyloid β−mediated brain disorder in a mouse model of Alzheimer disease. *J. Clin. Invest. 122*, 1377−1392.
(38) Ross, N. T., Deane, R., Perry, S., and Miller, B. L. (2013) Structure−activity relationships of small molecule inhibitors of RAGE-Aβ binding. *Tetrahedron 69*, 7653−7658.
(39) (a) Lue, L. F., Walker, D. G., Jacobson, S., and Sabbagh, M. (2009) Receptor for advanced glycation end products: its role in Alzheimer's disease and other neurological diseases. *Future Neurol. 4*, 167−177. (b) Lue, L.-F., Walker, D. G., Brachova, L., Beach, T. G., Rogers, R., Schmidt, A. M., Stern, D. M., and Yan, S. D. (2001) Involvement of microglial receptor for advanced glycation endproducts (RAGE) in Alzheimer's disease: identification of a cellular activation mechanism. *Exp. Neurol. 171*, 29−45. (c) Choi, B.-R., Cho, W.-H., Kim, J., Lee, H. J., Chung, C.-H., Jeon, W. K., and Han, J.-S. (2014) Increased expression of the receptor for advanced glycation end products in neurons and astrocytes in a triple transgenic mouse model of Alzheimer's disease. *Exp. Mol. Med. 46*, No. e75. (d) Sasaki, N., Toki, S., Chowei, H., Saito, T., Nakano, N., Hayashi, Y., Takeuchi, M., and Makita, Z. (2001) Immunohistochemical distribution of the receptor for the advanced glycation end products in neurons and astrocytes in Alzheimer's disease. *Brain Res. 888*, 256−262. (e) Miller, M. C., Tavares, R., Johanson, C. E., Hovanesian, V., Donahue, J. E., Gonzalez, L., Silverberg, G. D., and Stopa, E. G. (2008) Hippocampal RAGE immunoreactivity in early and advanced Alzheimer's disease. *Brain Res. 1230*, 273−280.
(40) Trott, O., and Olson, A. J. (2010) AutoDock Vina: improving the speed and accuracy of docking with a new scoring function, efficient optimization, and multithreading. *J. Comput. Chem. 31*, 455−461.
(41) Park, H., and Boyington, J. C. (2010) The 1.5 Å crystal structure of human receptor for advanced glycation endproducts (RAGE) ectodomains reveals unique features determining ligand binding. *J. Biol. Chem. 285*, 40762−40770.
(42) http://www.rcsb.org/pdb/explore.do?structureId=2MJW, accessed 19th November 2015.
(43) Penumutchu, S. R., Chou, R.-H., and Yu, C. (2014) Structural insights into calcium-bound S100P and the V domain of the RAGE complex. *PLoS One 9*, No. e103947.
(44) Buckley, S. T., and Ehrhadt, C. (2010) The receptor for advanced glycation end products (RAGE) and the lung. *J. Biomed. Biotechnol. 2010*, No. 917108.
(45) Logsdon, C. D., Fuentes, M. K., Huang, E. H., and Arumugam, T. (2007) RAGE and RAGE ligands in cancer. *Curr. Mol. Med. 7*, 777−789.
(46) Barlovic, D. P., Soro-Paavonen, A., and Jandeleit-Dahm, K. A. M. (2011) RAGE biology, atherosclerosis and diabetes. *Clin. Sci. 121*, 43−55.

DOI: 10.1021/acschemneuro.5b00319
ACS Chem. Neurosci. 2016, 7, 391−398